Published in final edited form as:
Virology. 2010 June 5; 401(2): 146–154. doi:10.1016/j.virol.2010.02.004.

Astrovirus infection induces sodium malabsorption and redistributes sodium hydrogen exchanger expression

Prashant K. Nighot[1], **Adam Moeser**[1], **Rizwana A. Ali**[2], **Anthony T. Blikslager**[1], and **Matthew D Koci**[2,*]

[1]Department of Clinical Sciences, North Carolina State University, Raleigh, NC

[2]Department of Poultry Science, North Carolina State University, Raleigh, NC

Abstract

Astroviruses are known to be a leading cause of diarrhea in infants and the immunocompromised; however, our understanding of this endemic pathogen is limited. Histological analyses of astrovirus pathogenesis demonstrate clinical disease is not associated with changes to intestinal architecture, inflammation, or cell death. Recent studies *in vitro* have suggested astroviruses induce actin rearrangement leading to loss of barrier function. The current study used the type-2 turkey astrovirus (TAstV-2) and turkey poult model of astrovirus disease to examine how astrovirus infection affects the ultrastructure and electrophysiology of the intestinal epithelium. These data demonstrate infection results in changes to the epithelial ultrastructure, rearrangement of F-actin, decreased absorption of sodium, as well as redistribution of the sodium/hydrogen exchanger 3 (NHE3) from the membrane to the cytoplasm. Collectively these data suggest astrovirus infection induces sodium malabsorption, possibly through redistribution of specific sodium transporters, which results in the development of an osmotic diarrhea.

Keywords

Astrovirus; Viral enteritis; Malabsorption diarrhea; Sodium/Hydrogen exchanger; Intestinal electrophysiology; Turkey

INTRODUCTION

Astroviruses are recognized as an endemic cause of acute gastroenteritis worldwide, with serologic studies demonstrating as high as 90% of individuals in some populations having anti-astrovirus antibodies (Glass *et al.*, 2001; Koopmans *et al.*, 1998). Astrovirus disease is typically associated with children under 2 years of age, and the immunocompromised. Clinically, astrovirus induces moderate-to-severe diarrhea, abdominal pain, and vomiting; however, astrovirus diarrhea is generally less severe than that caused by rotaviruses or noroviruses and rarely requires hospitalization (Walter and Mitchell, 2003). The fact that astrovirus infection rarely requires clinical intervention makes it difficult to determine its disease burden; however,

*Corresponding Author: Matthew Koci, Ph.D., Department of Poultry Science, North Carolina State University, Campus Box 7608, Raleigh, NC 27695, Office: 919.515.5388, Fax: 919.515.2625, mdkoci@ncsu.edu.

some investigators have estimated the total number of astrovirus-mediated episodes could be greater than those induced by noroviruses (Clark and McKendrick, 2004; Jakab et al., 2003).

In spite of its well recognized impact on human health, our understanding of how astroviruses cause disease is limited. This is largely due to the lack of an animal model to study the complex interactions between the virus and the intestinal epithelium. The majority of what is known about astrovirus pathogenesis has come from studies using the turkey model (Behling-Kelly et al., 2002; Koci et al., 2003; Thouvenelle, Haynes, and Reynolds, 1995; Thouvenelle et al., 1995). These experiments have demonstrated infection induces severe diarrhea in the absence of significant changes in the intestinal morphology. This includes a lack of changes in villus height, width, or surface area. Furthermore, there is no evidence of inflammation and no increase in cell death following astrovirus infection (Behling-Kelly et al., 2002; Koci et al., 2003; Thouvenelle, Haynes, and Reynolds, 1995). The lack of significant histological changes following infection has also been described in biopsy samples from astrovirus-infected children (Sebire *et al*., 2004).

Collectively, these observations indicate astroviruses induce diarrhea through a mechanism independent of viral-mediated destruction of the epithelium, leading some to speculate astroviruses affect the physiological function of intestinal epithelial cells. Recent *in vitro* studies examining the effect of astrovirus infection on Caco-2 cells have supported this hypothesis and suggest the astrovirus capsid protein alone can induce actin rearrangement, resulting in increased paracellular permeability and presumably diarrhea (Moser, Carter, and Schultz-Cherry, 2007).

To further understand how changes in the cellular ultrastructure are associated with clinical disease we examined the ultrastructural and electrophysiological changes of the intestinal epithelium using the type-2 turkey astrovirus (TAstV-2) animal model. The results of the present study are the first to our knowledge to examine the pathophysiology of astrovirus *in vivo* and indicate infection leads to changes in epithelial cell ultrastructure, including actin rearrangement, in the absence of electrophysiological evidence of changes in barrier permeability. Additionally, these data demonstrate infection induces malabsorption of Na^+ ions associated with redistribution of the Na^+/ H^+ exchanger, NHE3.

MATERIALS AND METHODS

Animals and viral Infection

One-day-old unvaccinated turkey poults were obtained from a commercial hatchery. Animals were randomly divided into 2 groups and placed in separate 934-1-WP isolators (L. H. Leathers Inc, Athens GA) with free access to feed and water. After an acclimation period of 3 days, one group was orally inoculated with ~10^6 genomic units of type-2 turkey astrovirus (TAstV-2/NC/99, TAstV-2) in 100 μl of phosphate-buffered saline (PBS) and one group sham inoculated (Con) with 100 μl of PBS as previously described (Koci *et al.*, 2003). The inoculum was previously determined to be the minimum dose resulting in 100% of challenged animals demonstrating virus replication within 24 hrs of inoculation (Behling-Kelly *et al.*, 2002). Animals were monitored daily for clinical signs. Samples of jejunum were collected at 4 days post infection (dpi) from 5 Con and 5 TAstV-2 infected animals for electrophysiology and unidirectional Na^+ and Cl^- flux studies on Ussing chambers, electronmicroscopy, and western blot analysis. Jejunal samples were also collected at 5 dpi for measuring paracellular mucosal-to-serosal ^{3}H-mannitol fluxes on Ussing chambers. These time points correspond with the onset of severe clinical signs.

All animal procedures were approved by the North Carolina State University Institutional Animal Care and Use Committee.

Electronmicroscopy

Jejunal tissues were fixed in McDowell's and Trump's 4F:1G fixative and processed for transmission electron microscopy using standard techniques (Dykstra, 1993). In brief, after 2 rinses in 0.1 M sodium phosphate buffer (pH 7.2), samples were placed in sodium phosphate buffer + 1% osmium tetroxide for 1hr at room temperature. Samples were rinsed 2 times in distilled water and dehydrated in an ethanolic series culminating in two changes of 100% acetone. Tissues were then placed in a mixture of Spurr's resin and acetone for 30 min, followed by 2 hr in 100% resin with 2 changes. Finally, samples were placed in fresh 100% resin in molds and polymerized at 70° C for 8 hrs to 3 days. Semi-thin (0.25–0.5 μ m) sections were cut with glass knives and stained with 1% toluidine blue-O in 1% sodium borate. Ultra thin (70–90 nm) sections were cut with a diamond knife, stained with methanolic uranyl acetate followed by lead citrate and examined with a transmission electron microscope (Phillips/ FEICO Model 208s).

Immunofluorescence

Jejunal tissues were embedded in OCT media (Tissue Tek, Sakura Finetek, Torrance CA), frozen, sectioned at 5 μm, and stored at −70° C until use. The sections were thawed, fixed in cold acetone, and incubated with a rabbit polycolonal antibody (anti-TAstV2nsp) generated to a peptide sequence derived from the TAstV-2 nonstructural protein (CAMEDRGEFYQKKSR, GenScript Corporation, Piscataway NJ). After washings in PBS, the sections were incubated in mixture of goat anti rabbit mouse-Alexa Fluor 488, phalloidin conjugated with Alexa fluor 546, and TO-PRO-3 (nucleic acid stain) (Invitrogen, Carlsbad CA). Slides were mounted in fluorescent mounting media (DakoCytomation) and examined with a Nikon Eclipse 2000E inverted microscope equipped with Nikon C1 confocal laser scanning system. Colocalization of the TAstVnsp antigen and F-actin immunofluorescence was analyzed using representative fields from 3 samples and the ImageJ program (http://rsb.info.nih.gov/ij/) using the colocalization finder plugin (Bolte and Cordelieres, 2006). Association of F-actin rearrangement with TAstV2nsp was further analyzed by overlaying the fluorescence images of TAstV-2 infected jejunum with a 25μm grid. Each grid was assessed for the presence or absence of TAstV2nsp fluorescence then separately analyzed for changes to F-actin within the grid. Changes in actin rearrangement were scored using a 3 point scale (1 = normal actin as determined by control tissues; 2 = moderate changes, 3 = severe changes). Three villi from three individual animals were analyzed and the percent distribution of the two parameters calculated.

Ussing chamber analysis

Immediately after euthanasia, the jejunum was harvested in oxygenated (95% O_2/5% CO_2) avian Ringer's solution (Whitsel, Johnson, and Forehand, 2002). The jejunal mucosa was stripped from the seromuscular layer and mounted in 1.3 cm^2 aperture Ussing chambers, as previously described (Argenzio and Liacos, 1990; Little et al., 2003). In subsequent experiments, whole jejunum was mounted on Ussing chambers to ensure changes in electrical parameters were not due to mechanical disruption resulting from stripping. For each Ussing chamber experiment, jejunal tissues from one animal were mounted on duplicate Ussing chambers. Tissues were bathed on the serosal and mucosal sides with 8 ml of oxygenated avian Ringer's solution circulated in water-jacketed reservoirs. The serosal bathing solution contained 10 mM glucose, and was balanced osmotically on the mucosal side with 10 mM mannitol. The spontaneous potential difference (PD) was measured using Ringer-agar bridges connected to calomel electrodes, and the PD was short-circuited through Ag-AgCl electrodes using a voltage clamp that corrected for fluid resistance to obtain measurements of short circuit current (I_{sc}). Transepithelial electrical resistance (TER, $\Omega \cdot cm^2$) was calculated from the

spontaneous potential difference and I_{sc}, as previously described (Blikslager, Roberts, and Argenzio, 1999; Little et al., 2003). I_{sc} and PD were recorded at 15 min intervals.

To study paracellular permeability, mucosal-to-serosal fluxes of [^{3}H]-mannitol were performed by adding [^{3}H]-mannitol (0.2 μCi/ml, diluted in 10 mM mannitol) to the mucosal side of Ussing chamber-mounted tissues. After a 15 min equilibration period, hot sample standards were taken from the mucosal side of each chamber. A 60 min flux period was established by taking 0.5 ml samples from the serosal compartment opposite to the mucosal compartment to which [^{3}H] mannitol was added. The presence of [^{3}H] was established by measuring β-emission in a liquid scintillation counter (1219 Rack Beta, LKB Wallac, Perkin Elmer, Waltham MA).

To assess transmucosal Na^+ and Cl^- fluxes, $^{22}Na^+$ or $^{36}Cl^-$ were added to the mucosal or serosal solutions of tissues paired according to their conductance (conductance within 25% of each other). After a 15 min equilibration period, standards were collected and 3 successive 30 min flux periods were performed by taking samples from the bathing reservoirs opposite the side of isotope addition. Data presented is from the second flux period. Samples were placed sequentially in β and γ liquid scintillation counters. The contribution of ^{22}Na β-counts to ^{36}Cl β-counts was subtracted and the unidirectional fluxes were calculated as previously described (Argenzio and Armstrong, 1993).

Western blotting

Jejunal mucosal scrapings from control and infected animals were snap frozen and stored at −70° C. Tissue aliquots were thawed at 4° C and added to chilled lysis buffer that included protease inhibitors (0.5 mM Pefabloc, 0.1 mM 4-nitrophenyl phosphate, 0.04 mM glycerophosphate, 0.1 mM $Na3VO_4$, 40 μg/ml bestatin, 2 μg/ml aprotinin, 0.54 μg/ml leupeptin, and 0.7 μg/ml pepstatin A). This mixture was homogenized on ice, centrifuged (800 × g for 10 min at 4° C) to remove debris, clarified by centrifugation (2,000 × g for 10 min at 4° C), a nd the supernatant collected. Protein concentrations were determined (BCA Protein Assay, Pierce, Rockford IL) and samples normalized based on total protein concentration.

To assay for differences in membrane or cytosolic cellular localization of protein, jejunal mucsoa scrapings were first homogenized in buffer (20 mM Tris, 5 mM $MgCl_2$, 0.3 mM EGTA, 210 μg/ml sodium fluoride, 18.5 μg/ml sodium orthovandate, 30 mM sodium pyrophosphate, and Complete Mini Protease inhibitor cocktail tablet (Pierce)) and centrifuged to remove debris (800 × g for 5 min at 4° C). Supernatants were then incubated for 30 min at 4° C with lysis buffer cont aining 0.5 % Triton X-100, centrifuged (120,000 × g for 30 min at 4° C) and supernatant co ntaining detergent soluble proteins collected (predominantly cytosolic proteins). The pellet was resuspended in lysis buffer containing 0.5 % SDS and processed as above to obtain detergent insoluble proteins (predominantly membrane proteins). Before SDS-PAGE analysis, samples were processed through a SDS-PAGE sample preparation kit to remove excessive detergent. Protein concentrations were determined (BCA Protein Assay, Pierce) and samples normalized based on total protein.

Samples for PAGE analysis were mixed with 4× XT sample buffer (Bio-Rad, Hercules CA) and boiled for 4 min. Lysates were loaded on a 4–12% Bis-Tris gels with XT MOPS buffer (Bio-Rad) and electrophoresis was performed. Proteins were transferred to a PVDF membrane (Millipore, Billerica MA), blocked at room temperature for 60 min in Tris-HCl buffer plus 0.05% Tween 20 (TBST) and 5% dry powdered milk and incubated overnight at 4° C with either rabbit polyclonal anti-NHE2 (Donowitz *et al.*, 1998) or anti-NHE3 (Hoogerwerf *et al.*, 1996), a generous gift from Dr. Mark Donowitz, Johns Hopkins University. Relative concentration of NHE2 and NHE3 were determined by densitometry and comparing band densities to β-actin (rabbit polyclonal anti-β-actin, Abcam Inc., MA) in each fraction as

previously described (Hayashi et al., 2004; Nighot et al., 2009; Swystun et al., 2009). Detergent soluble fraction and detergent insoluble fractions where confirmed to be enriched for cytoplasmic and membrane proteins respectively by assaying for lactate dehydrogenase and calnexin. There was no difference in expression of these two proteins between control and TAstV-2 infected tissues (data not shown). Proteins were detected using horseradish peroxidase-conjugated secondary antibody, and visualized with luminol enhancer solution (Pierce).

Determination of filamentous (F) and globular (G) actin was followed as described by Musch et al (2005). Briefly, intestinal mucosa was scrapped and extracted in actin stabilization buffer (Musch, Walsh-Reitz, and Chang, 2006). G-actin pool was separated by centrifugation (45,000 × *g*, 60 min, at 30° C), and F-actin pool was depolymerized with 1μM cytochalasin D. Following protein analysis with bicinchoninic acid procedure (Pierce), samples were solubilized with 4X sample XT buffer and western analysis (20 μg protein per lane) was performed as described above. Rabbit polyclonal anti-actin antibody (Cytoskeleton; Denver, CO) and horseradish peroxidase-conjugated secondary antibody was used for visualization of actin bands.

Statistical analysis

Data were reported as mean ± standard error (SE). All data were analyzed by using a Student's *t*-test for differences among groups (infected *vs*. sham-infected). $P < 0.05$ was considered significant.

RESULTS

Astrovirus-induced diarrhea occurs in the absence of histological and morphological changes

Previous studies in our laboratory and others have demonstrated astrovirus infection induces unremarkable histological changes which do not explain the severity of diarrhea (Behling-Kelly et al., 2002; Koci et al., 2003; Sebire et al., 2004; Snodgrass et al., 1979; Thouvenelle, Haynes, and Reynolds, 1995; Woode et al., 1984). The focus of the current study was to identify submicroscopic pathophysiological factors associated with astrovirus disease *in vivo*. To that end tissues from the current study were first examined to confirm no overt histological changes associated with the diarrhea.

Naïve animals were orally inoculated and monitored for signs of clinical disease and virus replication, as previously described (Koci *et al.*, 2003). Individually infected animals began demonstrating clinical signs (yellow, watery, and frothy diarrhea) within 24 hrs of inoculation. The numbers of animals presenting with clinical signs increased daily, with 100% of inoculated animals exhibiting diarrhea by 3 dpi (data not shown). The severity of clinical signs persisted for approximately 4 days followed by a recovery period which lasted until the end of the experiment. The kinetics of the clinical disease and correlation with the level of virus in intestinal samples and feces, as detected by real time RT-PCR (data not shown), was similar to previous reports (Koci *et al*., 2003).

At necropsy, the intestines of infected animals were found to be distended, and filled with frothy fluid, consistent with diarrheal disease. Hematoxylin and eosin staining and light microscopic examination of the duodenum, jejunum, ileum, and cecum demonstrated no notable changes between infected and control animals, including a lack of villus blunting, crypt hyperplasia or epithelial sloughing (Fig 1). Additionally, morphometric assessment of the villous height, villous width, villous surface area, crypt depth, villous height: crypt depth ratio, and number of goblet cells per villi revealed no significant differences between control and

TAstV-2 infected samples (data not shown). These observations were consistent with previous reports and demonstrate TAstV-2-induced diarrhea occurs without light microscopic mucosal changes (Behling-Kelly *et al.*, 2002;Koci *et al.*, 2003).

TAstV-2 infection results in ultrastructural changes and actin rearrangement in intestinal epithelial cells

To determine if astrovirus-induced clinical disease was associated with submicroscopic changes in the intestinal epithelium, sections of the jejunum were collected from control and infected animals at 4 dpi (12 – 24 hrs post onset of severe clinical signs in 100% of inoculated animals) and processed for analysis by TEM. TEM analysis demonstrated epithelium from control tissues had normal appearance with clearly demarcated tight junctions, whereas epithelium from TAstV-2 infected tissues had evidence of electron dense aggregates within the apical region of the enterocytes (Fig 2). These electron dense aggregates were more prominent in the epithelial cells at the tips of villi and were less frequently noted toward the intestinal crypts within the basal region of the mucosa (Fig 2). Electron dense aggregates did not appear to be specifically associated with tight junctions, and there was no evidence of paracellular dilatation in these regions (Fig 2). The electron dense aggregates appeared to be clustered around filaments extending from the microvilli, suggesting viral-induced alteration of the cytoskeleton.

To investigate if electron dense aggregates were associated with actin rearrangement, tissue sections were assayed for changes in F-actin using fluorescent-labeled phalloidin. F-actin in control tissues appeared as a sharp fluorescence demarcating individual enterocytes, with some evidence of intracellular stress fibers (Fig 3A). In contrast, the TAstV-2-infected jejunum revealed a poorly defined and thickened layer of F-actin fluorescence along the apical border of enterocytes with focal areas of aggregations (Fig 3A).

Analysis of tissues stained for both F-actin and TAstVnsp suggested a correlation between areas of the intestine positive for virus replication and areas with changes in F-actin (Fig 3A). To better assess this relationship tissues were analyzed to determine the percent of tissues where both events could be observed in the same 25μm grid. This analysis demonstrated TAstVnsp was found in approximately 80% of the tissue from infected animals, with approximately two thirds of these infected regions to have moderate to severe changes in actin (Fig 3B). More specifically, these fluorescent images were examined for colocalization of TAstV2nsp and F-actin. The results of these analyses demonstrated significant colocalization (Overlap coefficient = 0.98, $p<0.05$) between F-actin and TAstV2nsp fluorescence.

To further characterize the actin rearrangement observed in the TAstV-2 infected small intestinal epithelium, immunoblotting was employed to study total actin content and the proportion of G- and F-actin in TAstV-2 infected intestinal mucosa. The total actin content in mucosal homogenates, as assessed by pan-actin antibody staining, was not different in TAstV-2 infected tissue as compared to control tissues (data not shown). Moreover, the ratio of G- and F-actin was also found to be unchanged after TAstV-2 infection (data not shown). Thus the rearrangement of apical F-actin after TAstV-2 was found to be limited to morphological alterations without changes in actin content.

Ultrastructural changes are not associated with changes in mannitol permeability

To further characterize the pathophysiological significance of the ultrastructural changes, sections of jejunum were assayed for changes in paracellular permeability by assaying for differences in mucosal-to-serosal fluxes (J_{ms}) of [^{3}H]-mannitol across the jejunum of TAstV-2 infected and control animals. There was no significant difference between J_{ms} mannitol in control versus infected tissues (0.61 ±0.06 *vs*. 0.53±0.04 μmol/cm^2.h^{-1} respectively, $p > 0.05$);

however, conductance (G) was found to be increased in TAstV-2 infected animals as compared to controls (Table 1). This suggests that although macromolecular permeability was not altered, as measured by flux of mannitol, there were changes in permeability at the ionic level, as measured by G.

TAstV-2-associated change in ion transport

To further characterize the effect TAstV-2 infection had on the electrophysiological properties of the gut, jejunal sections were assayed for changes in ion transport as reflected by short circuit current (I_{sc}) and defined by unidirectional fluxes of Na^+ and Cl^- (Argenzio and Liacos, 1990; Blikslager, Roberts, and Argenzio, 1999; Li, Findlay, and Sheppard, 2004). The I_{sc} values of jejunum from infected animals did not indicate the presence of a typical electrogenic secretory response in which the principal ion secreted is anionic (Table 1). This was confirmed by analysis of the Na^+ and Cl^- transport. No significant differences in mucosal-to-serosal, serosal-to-mucosal, or net flux of Cl^- (Table 1) were observed. Additionally, no significant difference in serosal-to-mucosal flux of Na^+ was detected between the jejunum of control and infected animals (Table 1); however, mucosal-to-serosal Na^+ flux was significantly reduced in TAstV-2-infected animals. Accordingly, net Na^+ absorption was significantly reduced in TAstV-2-infected tissues (Table 1). These findings indicated that infection was associated with malabsorption of Na^+. Although Na^+ absorption is typically electroneutral (no change in I_{sc}), it is possible that Na^+ absorption was reduced to the extent that it contributed to changes in measurements of I_{sc} (Martinez-Augustin et al., 2009).

Dysregulation of sodium hydrogen exchangers in TAstV-2 infected animals

Based on the observations that TAstV-2 infection impaired absorption of Na^+, we assayed for changes in expression of sodium hydrogen exchangers (NHE). NHE2 and NHE3 have been described as the principal intestinal brush border NHE isoforms contributing to electroneutral Na^+ absorption in the avian small intestine (Donowitz *et al.*, 1998). To assay for their relative level of expression, western blot analyses of jejunal mucosal scrapings were performed. The level of NHE2 in whole tissue lysates was increased in the TAstV-2-infected animals as compared to controls (Fig 4D). Alternatively, there was no significant difference in the level of NHE3 protein (Fig 4A). These changes were difficult to interpret given our electrical findings, leading us to study NHE expression within cell fractions. Since NHE2 and NHE3 reside in the plasma membrane, we assayed for a difference in their expression in detergent soluble and detergent insoluble fractions. Detergent soluble fractions would be expected to contain proteins contained within the cytoplasm, whereas insoluble fractions would include the apical membrane in addition to other hydrophobic proteins. The results of these assays demonstrated a significant shift in the location of NHE3 within the cell following infection. The TAstV-2-infected tissues had approximately half the amount of NHE3 associated with the insoluble fraction as compared to the controls (Fig 4B and C). No significant difference was observed in the cellular localization of NHE2 (Fig 4E and F).

DISCUSSION

Understanding how viruses induce diarrhea and the specific changes to the host's intestinal physiology is essential to the development of more effective therapies. This is particularly important with a pathogen like astrovirus that has the heaviest disease burden in the immunologically immature and immunocompromised host. Previous studies of astrovirus pathogenesis in humans and animals suggest infection causes mild changes to the villus architecture, no change in absorptive surface area, and limited evidence of inflammation (Behling-Kelly et al., 2002; Koci et al., 2003; Sebire et al., 2004; Snodgrass et al., 1979; Thouvenelle, Haynes, and Reynolds, 1995; Woode et al., 1984). Studies by Thouvenelle et al suggested that astrovirus infection induces changes in expression of constituent proteins of the

brush border resulting in malabsorptive diarrhea; while more recent *in vitro* studies by Moser et al indicate astroviruses are capable of increasing paracellular permeability (Moser, Carter, and Schultz-Cherry, 2007; Thouvenelle et al., 1995). The present study was designed to identify astrovirus-mediated changes to the ultrastructure and electrophysiology of the small intestine which could help explain the mechanisms underlying clinical disease.

The present study focused on the jejunal region of the small intestine. The avian jejunum has been described to have more total surface area and is consequently a primary site of nutrient absorption as compared to other regions of the small intestine (Grubb and Bentley, 1990; Sklan et al., 2003). Additionally, previous studies have suggested astrovirus-induced changes to brush border enzyme activity may be greatest in the jejunum (Thouvenelle et al., 1995). Therefore we used the TAstV-2 and naïve turkey poult model to investigate astrovirus disease, including evaluation of electrophysiological parameters, mucosal-to-serosal mannitol fluxes, and unidirectional ion fluxes across the mucosa of the small intestine following the onset of severe clinical signs and virus replication. The present studies indicated that TAstV-2 infection induces malabsorption of Na^+. This malabsorption was accompanied by a decrease in expression of NHE3 in the detergent insoluble fraction and changes to the actin cytoskeleton associated with the epithelial brush border.

Na^+ malabsorption

Fluid loss into the intestinal lumen due to infectious diarrheal disease is primarily thought to involve electrogenic chloride secretion; while malabsorptive diarrheal disease typically refers to a reduction in absorptive surface area with which to absorb crucial electrolytes. The present study demonstrated neither appears to be involved with astrovirus-induced disease. These results demonstrated a malabsorption of Na^+ following infection. Reduced Na^+ absorption has been associated with infectious diarrhea (Halaihel et al., 2000; Shepherd et al., 1979), inflammatory bowel disease (Hawker, McKay, and Turnberg, 1980) and TNFα-induced experimental models of diarrhea (Clayburgh *et al.*, 2006). Impaired Na^+ absorption leads to a reduced gradient for water absorption due to accumulation of Na^+ in the lumen, causing malabsorptive diarrhea. What is particularly noteworthy in the present study is that astrovirus-induced diarrhea appears to be attributable to reduction in membrane expression of a Na^+ transporter associated with disruption of the apical membrane, which to our knowledge has not been previously identified as a mechanism for viral enteritis.

It should also be noted that Na^+ absorption however, is typically electroneutral (no change in I_{sc}) which was not the case here. Defects in the transport of ions other than Na^+ may also exist as the net Na^+ and Cl^- flux values did not fully explain the magnitude of change in I_{sc} in this study (Table 1), and thus the residual ion flux (not shown) could represent defects in other ion transport systems possibly as a result of the cell switching from electroneutral Na^+ absorption to electrogenic to compensate for the putative reduction in NHE3 activity (Flagella et al., 1999;Lucas, 2008). Additional studies are required to study other cations (K^+) or anions ($HCO3^-$) that contribute to changes in I_{sc}, and identify other ions whose transport across the intestinal barrier may also be disrupted.

Altered NHE expression

NHE2 and 3 belong to the *Slc9a* gene family which encodes nine NHE isoforms. Each isoform has been reported to be expressed differentially throughout the intestine and within the cell (Kiela, Xu, and Ghishan, 2006). NHE2 and 3 are thought to function almost exclusively in the apical membrane. They for the principle mechanism of enterocyte Na^+ absorption, and therefore form the basis of intestinal water absorption (Zachos, Tse, and Donowitz, 2005). NHE2 and 3 differ greatly as far as how their expression and activity is regulated within the cell. The NHE2 protein has been reported to be regulated transcriptionally (Cavet et al.,

2001) while NHE3 is regulated post-translationally through endosomal recycling (Akhter et al., 2002; Kurashima et al., 1998). Functionally, NHE3 is thought to be responsible for the majority of Na^+ absorption in mammals (Ledoussal et al., 2001; Wormmeester et al., 1998), while in the normal chicken ileum and colon NHE2 and NHE3 have been described to contribute equally to Na^+/H^+ exchange (Donowitz *et al.*, 1998). Expression and activity of these proteins however, have not been well characterized in the jejunum, and have not been studied in other avian species.

In the present study we found that although total expression of NHE3 was unchanged, its expression was increased in the detergent soluble fraction and decreased in the detergent insoluble fraction of TAstV-2-infected intestine. The decrease in detergent insoluble NHE3 in astrovirus-infected mucosa suggested a reduction in membrane expression of this protein. A decrease in NHE3 in the apical membrane would be expected to lead to a decrease in Na^+ absorption. In contrast, the total expression of NHE2 was increased in TAstV-2 infected jejunum. Although the reasons for these findings are not clear, increased expression of NHE2 in TAstV-2-infected jejunum could be a compensatory response for loss of NHE3 activity (Bachmann et al., 2004).

Previous studies to investigate the role of NHEs and Na^+ absorption during enteropathic *E. coli* (EPEC) infections have demonstrated a differential regulation of NHE2 and NHE3 (Hecht et al., 2004). The mechanisms involved in the differential regulation of NHE2 and 3 are not understood; however these differences are likely related to differences in how the proteins are regulated and differences in their cytoskeletal associations and membrane recycling.

Currently it is unclear if the changes in NHE3 expression following astrovirus infection are the result of specific targeting by viral proteins or a function of astrovirus-mediated changes to actin and/or interactions with other host proteins involved in linking NHE3 to the brush border. Initial studies to assay for changes in other proteins (NHERF, ezrin, ERK, etc) were unsuccessful due to a lack of cross-reactivity with turkey tissues. Efforts are presently underway to develop model specific reagents to further investigate the mechanisms involved in NHE3 inhibition.

Actin rearrangement and the epithelial barrier

The complexity of cytoskeletal-plasma membrane interactions is important for stabilization, function, and trafficking of transport proteins residing within the plasma membrane (Khurana, 2000). Apical F-actin forms a continuous ring around the epithelial cell that is anatomically linked to apical tight junctions and dynamically regulates tight junction permeability. For example, contraction of actin fibers opens the tight junctions and results in increased paracellular permeability (Madara, Moore, and Carlson, 1987; Turner et al., 1997).

The results of the experiments in the current study suggest astrovirus infection induced changes to the epithelial cytoskeleton *in vivo*. These changes in F-actin appeared at the apical surface as observed first as electron dense areas under TEM (Fig 2) and then subsequently by fluorescence (Fig 3). Moreover, the changes in F-actin were also observed to be associated with astrovirus replication, as detected by the presence of astrovirus non-structural protein (Fig 3). Colocalization of the F-actin and TAstV2nsp suggests that during astrovirus replication, nonstructural proteins localize to the apical region of the infected cell, potentially interacting with host proteins and affecting actin polymerization. The results of this study however, do not address what role other astrovirus proteins may play in the observed changes to F-actin. Previous studies have demonstrated astrovirus capsid protein alone is sufficient to induce changes in actin rearrangement *in vitro* (Moser, Carter, and Schultz-Cherry, 2007). Additional studies are necessary to better understand what effect specific astrovirus proteins and the different stages of the virus life cycle have on the enterocyte cytoskeleton.

The changes in epithelial actin were also associated with an increase in electrical conductance (Table 1) suggesting subtle changes in permability. However, there was no evidence of increased paracellular permeability as determined by mannitol fluxes or observation of changes in paracellular spaces as observed by TEM (Fig 2). Additionally, no changes in cellular localization of the tight junction protein ZO-1 was detected (data not shown). Collectively these results suggest infection was capable of inducing changes to the epithelial cytoskeleton, which in turn altered Na^+ transport and electrolyte permeability without inducing overt evidence of changes in barrier function.

These findings differ in some respects with those reported by Moser et al (2007) which reported that infection of Caco-2 cells with human astrovirus type-1 induced a loss of barrier function. The reason(s) for these differences is currently unclear; however, it could be a function of differences in the response of *in vivo* jejunal epithelial cells as compared to transformed colon cells (Caco-2 cells). Alternatively, the differences in changes to the epithelial cells could due to differences in stages of the virus infection at the time of analysis. The changes described by Moser et al occur within 36 hrs of infection *in vitro*, whereas in the current study intestinal epithelium was not sampled until after the onset of severe clinical signs (4dpi). Additional studies are needed to examine the kinetics of astrovirus-mediated changes in intestinal electrophysiology in the jejunum as well as other regions of the small intestine to better understand their association with and contribution to clinical disease.

Conclusion

These studies are the first, to our knowledge, to investigate the electrophysiological changes associated with astrovirus infection *ex vivo*. These results suggest astrovirus infection induced ultrastructural changes to the intestinal epithelium and rearrangement in F-actin. We hypothesize that these changes in actin disrupt the normal expression of transporter proteins in the apical membrane, specifically NHE3, and lead to malabsorption of Na^+, resulting in the failure to fully absorb water and ultimately clinical diarrhea. Future studies will investigate the specific interactions between astrovirus proteins, NHE3, and actin and their association with the severity of clinical disease, as well as the disruption of absorption of other ions and solutes.

Acknowledgments

The authors wish to thank Mrs Michelle Quiles and Ms Jessica Stall for technical support, the Laboratory for Advanced Electron and Light Optical Methods, CVM , NCSU for help with microscopy studies; Dr Jack Odle for help with animal laboratory facilities; and Mr Gerry Hammond for his help with the 934-1-WP Animal isolators. The 934-1-WP Animal isolators were developed for use at the USDA facility, Southeast Poultry Disease Research Lab, Athens, Georgia.

This work was supported in part by P30 DK34987 and the North Carolina Agricultural Foundation.

REFERENCES

Akhter S, Kovbasnjuk O, Li X, Cavet M, Noel J, Arpin M, Hubbard AL, Donowitz M. Na(+)/H(+) exchanger 3 is in large complexes in the center of the apical surface of proximal tubule-derived OK cells. Am J Physiol Cell Physiol 2002;283:C927–C940. [PubMed: 12176749]

Argenzio RA, Armstrong M. ANP inhibits NaCl absorption and elicits Cl secretion in porcine colon: evidence for cGMP and Ca mediation. Am J Physiol 1993;265:R57–R65. [PubMed: 8393628]

Argenzio RA, Liacos JA. Endogenous prostanoids control ion transport across neonatal porcine ileum in vitro. Am J Vet Res 1990;51:747–751. [PubMed: 2337271]

Bachmann O, Riederer B, Rossmann H, Groos S, Schultheis PJ, Shull GE, Gregor M, Manns MP, Seidler U. The Na+/H+ exchanger isoform 2 is the predominant NHE isoform in murine colonic crypts and its lack causes NHE3 upregulation. Am J Physiol Gastrointest Liver Physiol 2004;287:G125–G133. [PubMed: 14962844]

Behling-Kelly E, Schultz-Cherry S, Koci M, Kelley L, Larsen D, Brown C. Localization of astrovirus in experimentally infected turkeys as determined by in situ hybridization. Vet Pathol 2002;39:595–598. [PubMed: 12243474]

Blikslager AT, Roberts MC, Argenzio RA. Prostaglandin-induced recovery of barrier function in porcine ileum is triggered by chloride secretion. Am J Physiol 1999;276:G28–G36. [PubMed: 9886975]

Bolte S, Cordelieres FP. A guided tour into subcellular colocalization analysis in light microscopy. J Microsc 2006;224:213–232. [PubMed: 17210054]

Cavet ME, Akhter S, Murtazina R, Sanchez de Medina F, Tse CM, Donowitz M. Half-lives of plasma membrane Na(+)/H(+) exchangers NHE1-3: plasma membrane NHE2 has a rapid rate of degradation. Am J Physiol Cell Physiol 2001;281:C2039–C2048. [PubMed: 11698263]

Clark B, McKendrick M. A review of viral gastroenteritis. Curr Opin Infect Dis 2004;17:461–469. [PubMed: 15353966]

Clayburgh DR, Musch MW, Leitges M, Fu YX, Turner JR. Coordinated epithelial NHE3 inhibition and barrier dysfunction are required for TNF-mediated diarrhea in vivo. J Clin Invest 2006;116:2682–2694. [PubMed: 17016558]

Donowitz M, De La Horra C, Calonge ML, Wood IS, Dyer J, Gribble SM, De Medina FS, Tse CM, Shirazi-Beechey SP, Ilundain AA. In birds, NHE2 is major brush-border Na+/H+ exchanger in colon and is increased by a low-NaCl diet. Am J Physiol 1998;274:R1659–R1669. [PubMed: 9608021]

Dykstra, MJ. A manual of applied techniques for biological electron microscopy. New York: Plenum; 1993.

Flagella M, Clarke LL, Miller ML, Erway LC, Giannella RA, Andringa A, Gawenis LR, Kramer J, Duffy JJ, Doetschman T, Lorenz JN, Yamoah EN, Cardell EL, Shull GE. Mice lacking the basolateral Na-K-2Cl cotransporter have impaired epithelial chloride secretion and are profoundly deaf. J Biol Chem 1999;274:26946–26955. [PubMed: 10480906]

Glass RI, Bresee J, Jiang B, Gentsch J, Ando T, Fankhauser R, Noel J, Parashar U, Rosen B, Monroe SS. Gastroenteritis viruses: an overview. Novartis Found Symp 2001;238:5–19. [PubMed: 11444035]

Grubb BR, Bentley PJ. Potassium transport across the intestines of the fowl *Gallus domesticus*. J Comp Physiol B. 1990;160:17–22.

Halaihel N, Lievin V, Alvarado F, Vasseur M. Rotavirus infection impairs intestinal brush-border membrane Na(+)-solute cotransport activities in young rabbits. Am J Physiol Gastrointest Liver Physiol 2000;279:G587–G596. [PubMed: 10960359]

Hawker PC, McKay JS, Turnberg LA. Electrolyte transport across colonic mucosa from patients with inflammatory bowel disease. Gastroenterology 1980;79:508–511. [PubMed: 7429111]

Hayashi H, Szaszi K, Coady-Osberg N, Furuya W, Bretscher AP, Orlowski J, Grinstein S. Inhibition and redistribution of NHE3, the apical Na+/H+ exchanger, by Clostridium difficile toxin B. J Gen Physiol 2004;123:491–504. [PubMed: 15078917]

Hecht G, Hodges K, Gill RK, Kear F, Tyagi S, Malakooti J, Ramaswamy K, Dudeja PK. Differential regulation of Na+/H+ exchange isoform activities by enteropathogenic E. coli in human intestinal epithelial cells. Am J Physiol Gastrointest Liver Physiol 2004;287:G370–G378. [PubMed: 15075254]

Hoogerwerf WA, Tsao SC, Devuyst O, Levine SA, Yun CH, Yip JW, Cohen ME, Wilson PD, Lazenby AJ, Tse CM, Donowitz M. NHE2 and NHE3 are human and rabbit intestinal brush-border proteins. Am J Physiol 1996;270:G29–G41. [PubMed: 8772498]

Jakab F, Walter JE, Berke T, Matson DO, Mitchell DK, Szucs G. Molecular characterization and sequence analysis of human astroviruses circulating in Hungary. FEMS Immunol Med Microbiol 2003;39:97–102. [PubMed: 14625092]

Khurana S. Role of actin cytoskeleton in regulation of ion transport: examples from epithelial cells. J Membr Biol 2000;178:73–87. [PubMed: 11083897]

Kiela PR, Xu H, Ghishan FK. Apical NA+/H+ exchangers in the mammalian gastrointestinal tract. J Physiol Pharmacol 2006;57:51–79. [PubMed: 17228096]

Koci MD, Moser LA, Kelley LA, Larsen D, Brown CC, Schultz-Cherry S. Astrovirus induces diarrhea in the absence of inflammation and cell death. J Virol 2003;77:11798–11808. [PubMed: 14557664]

Koopmans MP, Bijen MH, Monroe SS, Vinje J. Age-stratified seroprevalence of neutralizing antibodies to astrovirus types 1 to 7 in humans in The Netherlands. Clin Diagn Lab Immunol 1998;5:33–37. [PubMed: 9455876]

Kurashima K, Szabo EZ, Lukacs G, Orlowski J, Grinstein S. Endosomal recycling of the Na+/H+ exchanger NHE3 isoform is regulated by the phosphatidylinositol 3-kinase pathway. J Biol Chem 1998;273:20828–20836. [PubMed: 9694828]

Ledoussal C, Woo AL, Miller ML, Shull GE. Loss of the NHE2 Na(+)/H(+) exchanger has no apparent effect on diarrheal state of NHE3-deficient mice. Am J Physiol Gastrointest Liver Physiol 2001;281:G1385–G1396. [PubMed: 11705743]

Li H, Findlay IA, Sheppard DN. The relationship between cell proliferation, Cl-secretion, and renal cyst growth: a study using CFTR inhibitors. Kidney Int 2004;66:1926–1938. [PubMed: 15496164]

Little D, Dean RA, Young KM, McKane SA, Martin LD, Jones SL, Blikslager AT. PI3K signaling is required for prostaglandin-induced mucosal recovery in ischemia-injured porcine ileum. Am J Physiol Gastrointest Liver Physiol 2003;284:G46–G56. [PubMed: 12388204]

Lucas ML. Enterocyte chloride and water secretion into the small intestine after enterotoxin challenge: unifying hypothesis or intellectual dead end? J Physiol Biochem 2008;64:69–88. [PubMed: 18663997]

Madara JL, Moore R, Carlson S. Alteration of intestinal tight junction structure and permeability by cytoskeletal contraction. Am J Physiol 1987;253:C854–C861. [PubMed: 3425707]

Martinez-Augustin O, Romero-Calvo I, Suarez MD, Zarzuelo A, de Medina FS. Molecular bases of impaired water and ion movements in inflammatory bowel diseases. Inflamm Bowel Dis 2009;15:114–127. [PubMed: 18626965]

Moser LA, Carter M, Schultz-Cherry S. Astrovirus increases epithelial barrier permeability independently of viral replication. J Virol 2007;81:11937–11945. [PubMed: 17699569]

Musch MW, Walsh-Reitz MM, Chang EB. Roles of ZO-1, occludin, and actin in oxidant-induced barrier disruption. Am J Physiol Gastrointest Liver Physiol 2006;290:G222–G231. [PubMed: 16239402]

Nighot PK, Moeser AJ, Ryan KA, Ghashghaei T, Blikslager AT. ClC-2 is required for rapid restoration of epithelial tight junctions in ischemic-injured murine jejunum. Exp Cell Res 2009;315:110–118. [PubMed: 18976652]

Sebire NJ, Malone M, Shah N, Anderson G, Gaspar HB, Cubitt WD. Pathology of astrovirus associated diarrhoea in a paediatric bone marrow transplant recipient. J Clin Pathol 2004;57:1001–1003. [PubMed: 15333670]

Shepherd RW, Butler DG, Cutz E, Gall DG, Hamilton JR. The mucosal lesion in viral enteritis. Extent and dynamics of the epithelial response to virus invasion in transmissible gastroenteritis of piglets. Gastroenterology 1979;76:770–777. [PubMed: 217794]

Sklan D, Geyra A, Tako E, Gal-Gerber O, Uni Z. Ontogeny of brush border carbohydrate digestion and uptake in the chick. Br J Nutr 2003;89:747–753. [PubMed: 12828791]

Snodgrass DR, Angus KW, Gray EW, Menzies JD, Paul G. Pathogenesis of diarrhoea caused by astrovirus infections in lambs. Arch Virol 1979;60:217–226. [PubMed: 116623]

Swystun VA, Renaux B, Moreau F, Wen S, Peplowski MA, Hollenberg MD, MacNaughton WK. Serine proteases decrease intestinal epithelial ion permeability by activation of protein kinase Czeta. Am J Physiol Gastrointest Liver Physiol 2009;297:G60–G70. [PubMed: 19460843]

Thouvenelle ML, Haynes JS, Reynolds DL. Astrovirus infection in hatchling turkeys: histologic, morphometric, and ultrastructural findings. Avian Dis 1995;39:328–336. [PubMed: 7677654]

Thouvenelle ML, Haynes JS, Sell JL, Reynolds DL. Astrovirus infection in hatchling turkeys: alterations in intestinal maltase activity. Avian Dis 1995;39:343–348. [PubMed: 7677656]

Turner JR, Rill BK, Carlson SL, Carnes D, Kerner R, Mrsny RJ, Madara JL. Physiological regulation of epithelial tight junctions is associated with myosin light-chain phosphorylation. Am J Physiol 1997;273:C1378–C1385. [PubMed: 9357784]

Walter JE, Mitchell DK. Astrovirus infection in children. Curr Opin Infect Dis 2003;16:247–253. [PubMed: 12821816]

Whitsel AI, Johnson CB, Forehand CJ. An in ovo chicken model to study the systemic and localized teratogenic effects of valproic acid. Teratology 2002;66:153–163. [PubMed: 12353211]

Woode GN, Pohlenz JF, Gourley NE, Fagerland JA. Astrovirus and Breda virus infections of dome cell epithelium of bovine ileum. J Clin Microbiol 1984;19:623–630. [PubMed: 6429189]

Wormmeester L, Sanchez de Medina F, Kokke F, Tse CM, Khurana S, Bowser J, Cohen ME, Donowitz M. Quantitative contribution of NHE2 and NHE3 to rabbit ileal brush-border Na+/H+ exchange. Am J Physiol 1998;274:C1261–C1272. [PubMed: 9612213]

Zachos NC, Tse M, Donowitz M. Molecular physiology of intestinal Na+/H+ exchange. Annu Rev Physiol 2005;67:411–443. [PubMed: 15709964]

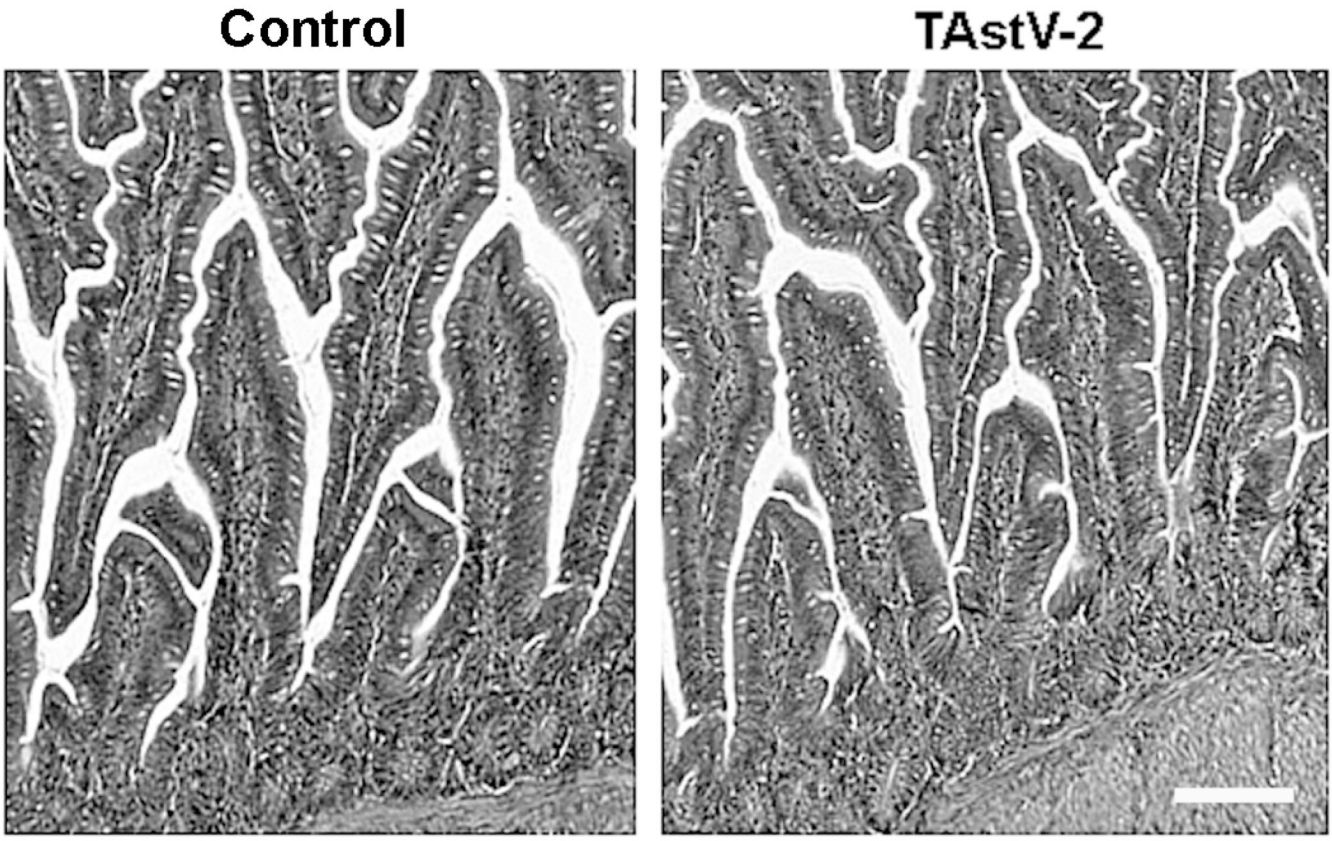

Fig 1. No evidence of histological changes following infection with TAstV-2

Sections of jejunum were collected from control and TAstV-2 infected poults at 4 dpi. Tissues were fixed in 10% buffered formalin, embedded in paraffin, sectioned, stained using H&E, and examined using light microscopy. White bar = 100μM. Panels are representative fields from 4 individuals per group.

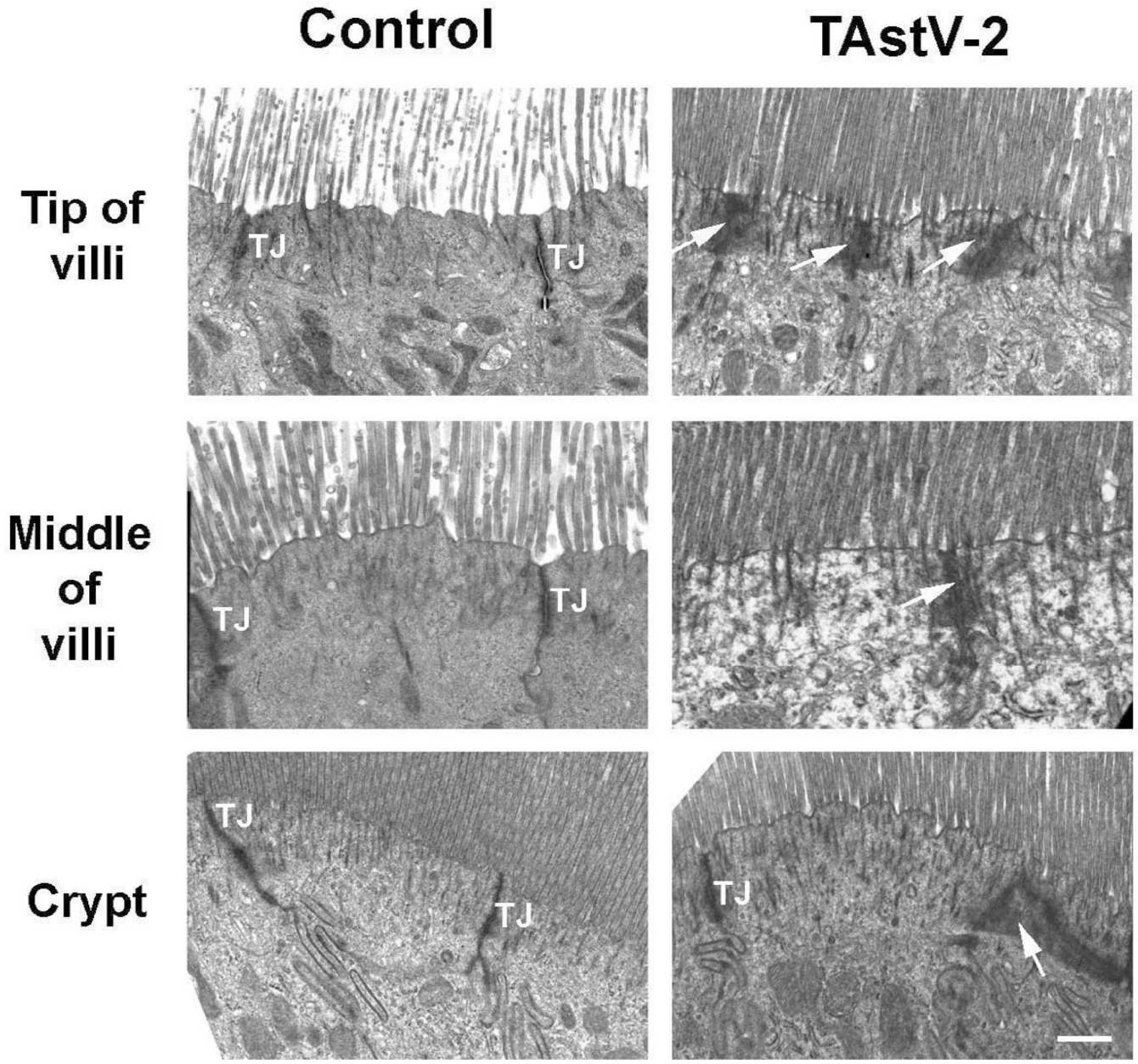

Fig 2. TAstV-2 infection mediated changes to the apical ultrastructure of epithelial cells

Jejunum from control and TAstV-2 infected animals were collected at 4 dpi and analyzed by transmission electronic microscopy at the tip of villi, middle of villi, and the crypts. Normal tight junctions (TJ) are demarcated in the control micrographs, while electron dense aggregations (arrows) were observed in the TAstV-2-infected jejunum. White bar represents 0.5 μM

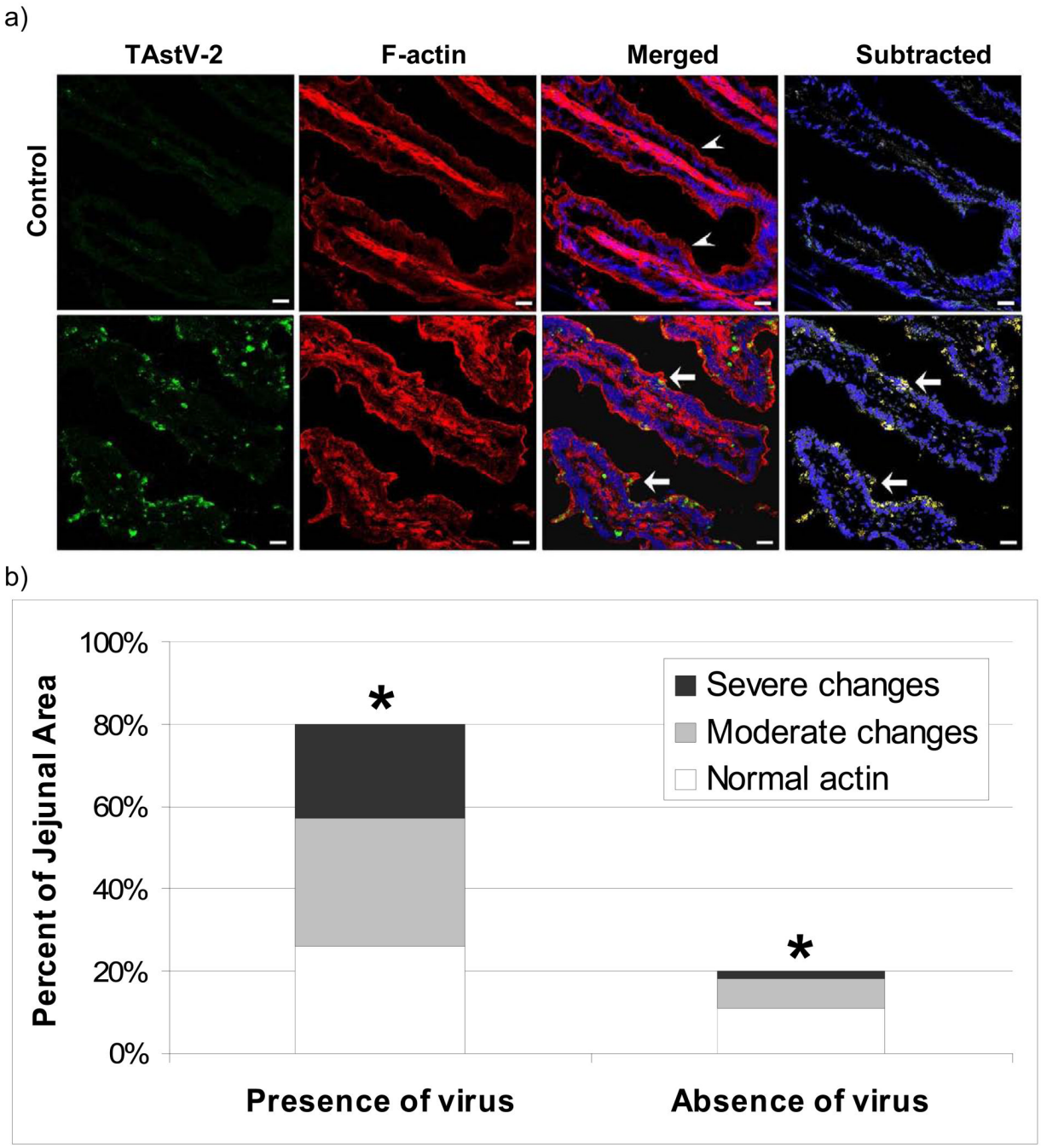

Fig 3. Actin reorganization following TAstV-2 infection

(A) Control and TAstV-2-infected jejunum sections collected at 4 dpi were stained for F-actin using phalloidin conjugated with Alexa fluor 546 (red), TAstV-2 nonstructural protein (green) and nuclei (blue), as detailed in methods. Arrow heads denote normal apical F-actin fluorescence, while arrows denote areas of rearrangement in actin. F-actin reorganization was prominent in the areas of virus localization (yellow color in merged panel). White bar represents 50μm. (B) Fluorescence images from TAstV-2 infected tissues were overlaid with a 25 μm grid. Individual grids were scored for actin rearrangement (normal/comparable with control tissues, moderate changes, severe changes). Grids were then assessed for the presence or absence of astrovirus fluorescence within the infected epithelium. Three villi, from 3 different

samples were analyzed. The percent distribution of both parameters was calculated and means represented by bars. * denotes significant difference $p < 0.001$ between changes in actin in grids with TAstV-2 and grids without.

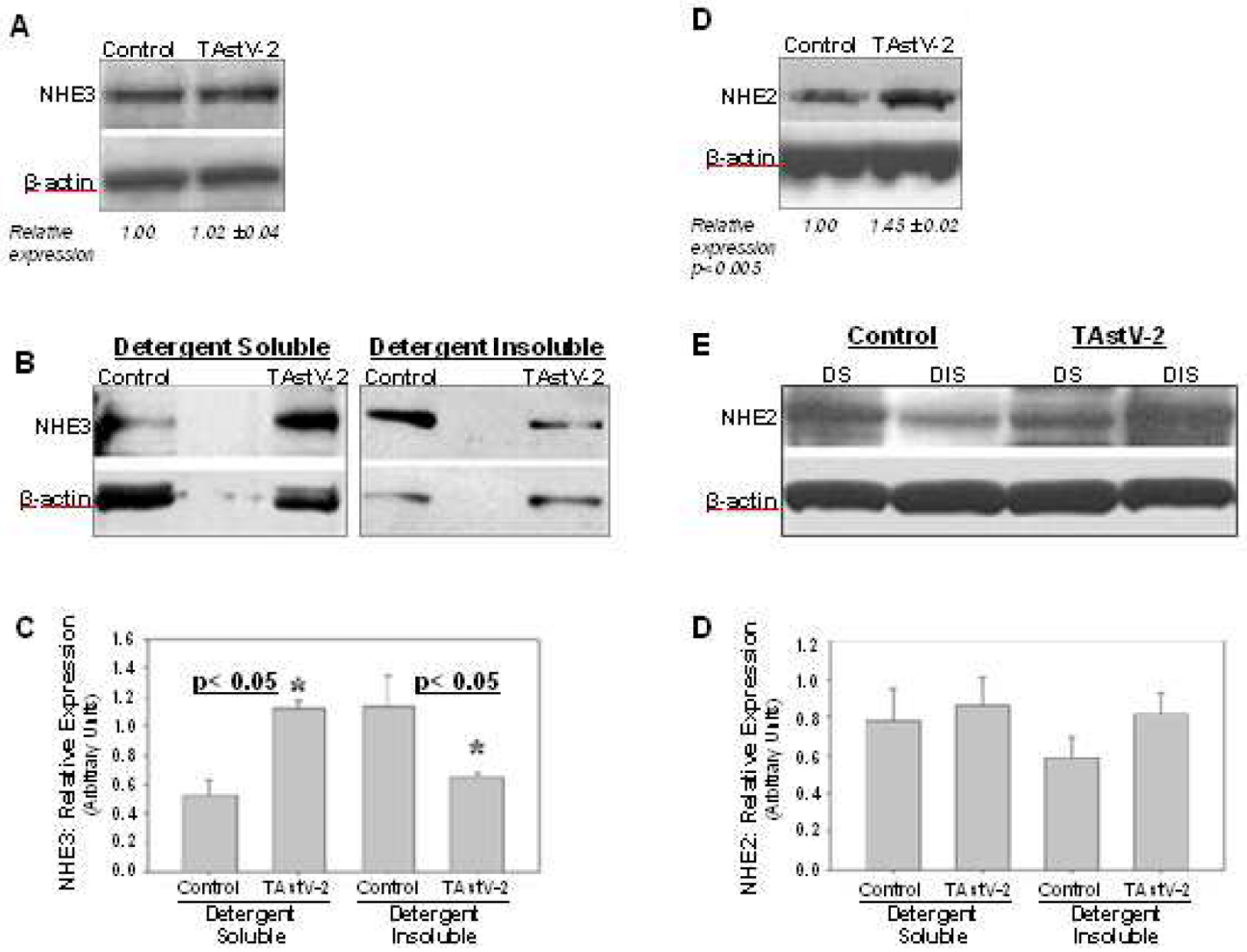

Fig 4. Cellular expression of NHE protein changes following TAstV-2 infection

Expression of sodium hydrogen exchangers (NHEs) in control and TAstV-2-infected jejunum at 4 days post infection was examined in whole tissue lysates (A and D) or detergent soluble (DS) and detergent insoluble (DIS) fractions (B, C, E, and F) as detailed in materials and methods section. Both NHE2 and NHE3 were identified as a single band of approximately 87 kd mass on western blots. β-actin bands are shown as loading controls for respective lanes in all blots. The densitometric data for NHE3 and NHE2 expression (NHE/β-actin) in whole tissue lysates is presented as mean ± SE in panel A and D. The densitometric data for NHE3 and NHE2 expression (NHE/β-actin) in detergent fractions is presented in panel C and F, respectively. All blots are representative of 3 or more experiments.

Table 1

A: Unidirectional Na^+ and Cl^- fluxes across stripped jejunum of control and TAstV-2 infected poults

	Na^+ Flux			Cl^- Flux				
	$J_{m\rightarrow s}$	$J_{s\rightarrow m}$	J_{Net}	$J_{m\rightarrow s}$	$J_{s\rightarrow m}$	J_{net}	*I*sc	G_t
Control	4.53±0.31	3.58±0.38	0.96±0.38	2.67±0.22	3.23±0.38	−0.56±0.40	9.40±0.9	9.33±0.9
TAstV-2	2.03±0.36*	4.13±0.42	−2.10±0.43*	2.70±0.40	2.26±0.39	0.44±0.37	4.00±1.7*	15.50±1.3*

B: Unidirectional Na^+ and Cl^- fluxes across intact jejunum of control and TAstV-2 infected poults

	Na^+ Flux			Cl^- Flux				
	$J_{m\rightarrow s}$	$J_{s\rightarrow m}$	J_{Net}	$J_{m\rightarrow s}$	$J_{s\rightarrow m}$	J_{net}	Isc	G_t
Control	4.36±0.48	3.80±0.29	0.57±0.53	1.72±0.44	2.14±0.38	−0.42±0.21	6.66±0.9	9.83±1.7
TAstV-2	2.91±0.27*	4.04±0.61	−1.13±0.54*	2.54±0.61	1.88±0.54	0.66±0.44	3.30±1.1*	17.50±1.4*

Values are mean ± SE. Jejunal tissue was stripped off seromuscular layer (A) or not (B) before mounting on Ussing chambers. Na^+ and Cl^- fluxes (J) and short-circuit current (I_{SC}) are given in µeq.cm^{-2}.h^{-1}, and tissue conductance (G_t) is given in mS/cm^2. $J_{M\rightarrow S}$, mucosal-to-serosal flux; $J_{s\rightarrow m}$, Serosal-to-mucosal flux; J_{net}, net flux. n= 6 for each experiment.

*$P < 0.05$ infected vs. control tissues (*t*-test).